Phytochemical-Assisted GreenSynthesis of Bismuth Oxide Nanoparticles Using *DesmodiumUnifoliatum*:Structural Characterization and Multifunctional Performance

13

P. Naveen
Dr. Gopi Mamidi
Dr. A. Indira Priyadarsini
Dr. G. Swathi

Abstract

A sustainable green route for the synthesis of bismuth oxide (Bi_2O_3) nanoparticles was developed using the aqueous leaf extract of Desmodium unifoliatum (Fabaceae) as a natural reducing and stabilizing agent. To the best of our knowledge, this is the first report describing the utilization of D. unifoliatum for the fabrication of Bi_2O_3 nanostructures. Phytochemicals present in the extract, including phenolics, flavonoids, and alkaloids, facilitated the reduction of Bi^{3+} ions and subsequent formation of Bi_2O_3 under mild reaction conditions. Optimization of synthesis parameters such as pH, temperature, and extract-to-precursor ratio resulted in crystalline á-Bi_2O_3 nanoparticles with an average crystallite size of 38 nm as estimated from XRD, and particle sizes in the range of 35–45 nm as observed by TEM. UV–visible spectroscopy showed a characteristic absorption band at 340 nm, while FTIR analysis confirmed the involvement of hydroxyl and carbonyl functional

P. Naveen
Lecturer in Chemistry, Government Degree College (Autonomous), Nagari, A.P., India, *Email; naveen.sklm@gmail.com*
Dr. Gopi Mamidi
Lecturer in Chemistry, Dr. V.S.K. Government Degree College, Visakhapatnam, A.P., India
Dr. A. Indira Priyadarsini
Lecturer in Botany, Government Degree College (Autonomous), Nagari, A.P., India
Dr. G. Swathi
Lecturer in Zoology, Government Degree College (Autonomous), Nagari, A.P., *India*
Publisher: Anu Books
Book Name : Chemical Sciences at the Nexus of Sustainability: Bridging Disciplines

groups along with Bi–O vibrations. The nanoparticles exhibited a negative zeta potential (-25.4 mV), indicating good colloidal stability, and DLS analysis revealed a hydrodynamic diameter of 48 ± 4 nm. Elemental purity was confirmed by EDX analysis. The synthesized Bi_2O_3 nanoparticles demonstrated notable antibacterial activity against Staphylococcus aureus (18 mm) and Escherichia coli (16 mm), significant antioxidant activity with 76.3% DPPH radical scavenging efficiency, and effective photocatalytic degradation of methylene blue (84% within 120 min, k = 0.014 min^{-1}). Comparative evaluation with previously reported green-synthesized Bi_2O_3 systems indicates that D. unifoliatum-mediated nanoparticles possess a smaller size, good stability, and multifunctional performance.

This study identifies Desmodium unifoliatum as a new phytochemical resource for the green synthesis of Bi_2O_3 nanoparticles. The multifunctional properties of the synthesized nanoparticles suggest their potential applicability in antimicrobial coatings, antioxidant systems, and visible-light-driven environmental remediation.

Keywords: *Desmodium unifoliatum; Bi_2O_3 nanoparticles; green synthesis; antioxidant activity; antibacterial activity; photocatalysis; dynamic light scattering.*

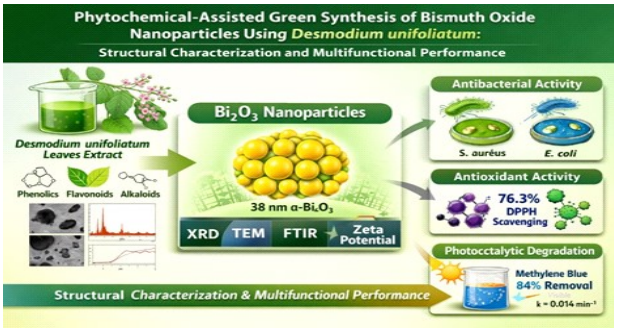

1. Introduction

1.1. Background

Nanotechnology has enabled precise control over material properties at the nanoscale, leading to enhanced optical, catalytic, electronic, and biological functionalities compared to bulk counterparts [1–3]. Among nanomaterials, metal oxide nanoparticles have attracted considerable attention due to their chemical stability, tunable band gaps, and applicability in environmental remediation, biomedical devices, and energy-related applications [4,5]. Bismuth oxide (Bi_2O_3) is a p-type semiconductor with a relatively narrow band gap (2.7–2.9 eV), enabling visible-light-driven activity suitable for photocatalysis, antimicrobial coatings, and sensing applications [6–9]. Additionally, Bi_2O_3 exhibits low toxicity and a high refractive index, supporting its use in optical devices and radiation shielding materials [10]. Conventional synthesis techniques for Bi_2O_3 nanoparticles, including

sol–gel, hydrothermal, and chemical precipitation methods, often involve high temperatures, strong alkaline conditions, or hazardous chemicals, raising concerns regarding environmental impact and scalability [11,12]. Consequently, the development of environmentally benign and cost-effective synthesis strategies has become an important focus in current nanomaterials research [13].

1.2. Green Synthesis and Mechanistic Considerations

Green synthesis approaches utilize biological resources such as plants, microorganisms, and biopolymers to replace toxic reducing and stabilizing agents [14–16]. Plant-mediated synthesis is particularly advantageous due to the abundance of bioactive phytochemicals-polyphenols, flavonoids, tannins, terpenoids, and proteins—which act as electron donors and stabilizers during nanoparticle formation [17–19]. Compared to microbial methods, plant-based systems offer faster synthesis, simpler processing, and improved nanoparticle stability [20]. Despite these advantages, reports on green synthesis of Bi_2O_3 nanoparticles remain limited [21]. Existing studies using plant extracts such as *Aloe vera*, *Azadirachta indica*, and *Citrus sinensis* often report relatively larger particle sizes and provide limited insight into structure–property relationships [22–24]. Therefore, the exploration of new plant systems capable of producing stable and well-defined Bi_2O_3 nanoparticles remains necessary.

1.3. *Desmodium unifoliatum* as a Phytochemical Resource

Desmodium unifoliatum (Fabaceae) is a medicinal plant native to the Seshachalam Hills region of Andhra Pradesh, India, and is traditionally used for its anti-inflammatory, antioxidant, and hepatoprotective properties [25,26]. Phytochemical investigations have reported the presence of flavonoids, phenolic acids, alkaloids, terpenoids, and saponins, which exhibit strong metal-chelating and reducing capabilities [27,28]. Despite its medicinal relevance, *D. unifoliatum* has not been previously explored for nanoparticle synthesis. Its unique phytochemical profile provides a strong rationale for investigating its potential role in the green synthesis of Bi_2O_3 nanoparticles.

1.4. Research Gap and Objectives

Although green synthesis methods are increasingly reported, a clear understanding of the relationship between plant phytochemistry, synthesis parameters, and functional performance of Bi_2O_3 nanoparticles remains incomplete [29,30]. The present study aims to address this gap by investigating *D. unifoliatum* leaf extract as a reducing and stabilizing agent for Bi_2O_3 nanoparticle synthesis.

The objectives of this study are to:

- Develop a green synthesis route for Bi_2O_3 nanoparticles using *D. unifoliatum* leaf extract.

- Identify key phytochemical components involved in reduction and stabilization.
- Optimize synthesis parameters to control nanoparticle size and morphology.
- Characterize the synthesized nanoparticles using standard physicochemical techniques.
- Evaluate antibacterial, antioxidant, and photocatalytic activities.
- Compare the performance of the synthesized nanoparticles with previously reported green-synthesized Bi_2O_3 systems.

2. Materials and Methods

2.1. Materials and Reagents

All chemicals used in this study were of analytical grade and were used without further purification. Bismuth nitrate pentahydrate ($Bi(NO_3)_3 \cdot 5H_2O$), sodium hydroxide (NaOH), ethanol (99.9%), methylene blue (MB), and 2,2-diphenyl-1-picrylhydrazyl (DPPH) were purchased from Sigma–Aldrich, India. Folin–Ciocalteu reagent, gallic acid, and quercetin were procured from HiMedia Laboratories, Mumbai, India. Deionized water with a resistivity of 18.2 MΩ·cm was used throughout all experimental procedures. All glassware was thoroughly cleaned using 10% (v/v) nitric acid solution and rinsed repeatedly with deionized water prior to use [31]. Microbial strains *Staphylococcus aureus* (MTCC 3160, Gram-positive) and *Escherichia coli* (MTCC 1687, Gram-negative) were obtained from the Microbial Type Culture Collection (MTCC), Chandigarh, India, and were maintained according to standard laboratory protocols.

2.2. Plant Collection and Authentication

Fresh, mature leaves of *Desmodium unifoliatum* were collected from the hilly regions surrounding Nagari, Chittoor District, Andhra Pradesh, India (13.320° N, 79.580° E), during the monsoon season (July 2025). The collected plant material was authenticated and taxonomically identified at the Department of Botany, Government Degree College (Autonomous), Nagari. A voucher specimen (No. DU/NAG/2025/07) was deposited in the institutional herbarium for future reference (25,26). The collected leaves were thoroughly washed with tap water, followed by distilled water to remove adhering dust and surface impurities. The cleaned leaves were shade-dried at ambient temperature for seven days, ground into a fine powder using a mechanical grinder, and stored in an airtight container until further use.

2.3. Preparation of Aqueous Leaf Extract

Ten grams of the powdered *Desmodium unifoliatum* leaves were mixed with 100 mL of deionized water in a 250 mL Erlenmeyer flask and heated at 95 °C

for 15 min with constant stirring at 500 rpm. After heating, the mixture was allowed to cool to room temperature and was filtered through Whatman No. 1 filter paper. The filtrate was centrifuged at 6000 rpm for 10 min to remove insoluble plant debris, and the clear supernatant was collected. The aqueous extract was stored at 4 °C and used within 24 h to ensure phytochemical stability [27].

2.4. Phytochemical Screening of *Desmodium unifoliatum* Extract

2.4.1. Qualitative Analysis

Standard qualitative phytochemical tests were performed following established procedures to identify the major classes of secondary metabolites present in the aqueous leaf extract [28,29]. Alkaloids were detected using Mayer's and Dragendorff's reagents, where the formation of cream or orange precipitates indicated a positive result. Flavonoids were identified by the alkaline reagent test, evidenced by the development of a yellow coloration that disappeared upon acidification. The presence of tannins and phenolic compounds was confirmed using the ferric chloride test, which produced a blue–green coloration. Saponins were detected by the frothing test, indicated by the formation of persistent foam greater than 1 cm in height. Terpenoids were identified using the Salkowski test, where the appearance of a reddish-brown interface confirmed their presence.

2.4.2. Quantitative Estimation

Quantitative estimation of phytochemical constituents was carried out using standard spectrophotometric methods. Total phenolic content (TPC) was determined using the Folin–Ciocalteu assay at 765 nm and expressed as gallic acid equivalents (GAE). Total flavonoid content (TFC) was measured by the aluminum chloride colorimetric method at 415 nm and expressed as quercetin equivalents (QE). Total tannin content was estimated using the vanillin assay at 500 nm and expressed as tannic acid equivalents (TAE) [30].

2.5. Green Synthesis of Bi_2O_3 Nanoparticles

For the synthesis of Bi_2O_3 nanoparticles, 50 mL of 0.01 M bismuth nitrate pentahydrate ($Bi(NO_3)_3 \cdot 5H_2O$) solution was mixed with 50 mL of *Desmodium unifoliatum* leaf extract in a 1:1 (v/v) ratio under continuous magnetic stirring at 600 rpm. The pH of the reaction mixture was adjusted to 9.0 using 0.1 M NaOH solution to facilitate metal ion reduction and oxide formation. The reaction was maintained at 70 °C for 2 h, during which the color of the solution gradually changed from pale yellow to dark brown, indicating nanoparticle formation. After completion of the reaction, the mixture was allowed to cool to room temperature. The resulting suspension was centrifuged at 8000 rpm for 10 min, and the collected precipitate was washed three

times with deionized water followed by ethanol to remove unbound phytochemical residues. The purified product was dried at 80 °C overnight and subsequently calcined at 400 °C for 2 h to obtain crystalline Bi_2O_3 nanoparticles [32].

2.6. Optimization of Reaction Parameters

Optimization of the synthesis process was carried out by varying one reaction parameter at a time while keeping all other parameters constant. The pH of the reaction mixture was varied in the range of 6–10, the reaction temperature was adjusted between 50 and 80 °C, and the extract-to-precursor volume ratio was varied from 0.5:1 to 2:1. The influence of each parameter on nanoparticle formation was evaluated using UV–visible spectroscopy by monitoring changes in absorbance intensity and peak position. Particle size and dispersion stability were further assessed using TEM, DLS, and zeta potential measurements to determine the optimum synthesis conditions [33].

2.7. Characterization Techniques

2.7.1. UV–Visible Spectroscopy

The optical properties and formation of Bi_2O_3 nanoparticles were analyzed using a Shimadzu UV-1800 UV–visible spectrophotometer in the wavelength range of 200–800 nm. The characteristic absorption band observed near 340 nm was used to confirm the formation of Bi_2O_3 nanoparticles and the reduction of Bi^{3+} ions [34].

2.7.2. Fourier Transform Infrared (FTIR) Spectroscopy

FTIR spectra of the *Desmodium unifoliatum* extract and synthesized Bi_2O_3 nanoparticles were recorded using a PerkinElmer Spectrum Two FTIR spectrometer in attenuated total reflectance (ATR) mode. Spectra were collected in the range of 400–4000 cm^{-1} with a resolution of 4 cm^{-1} and 32 scans. Functional groups involved in nanoparticle reduction and stabilization were identified by comparing the spectra before and after synthesis [35].

2.7.3. X-Ray Diffraction (XRD)

The crystalline phase and structural properties of the synthesized Bi_2O_3 nanoparticles were determined using a Bruker D8 Advance X-ray diffractometer with Cu Kα radiation (λ = 1.5406 Å). Diffraction patterns were recorded over a 2θ range of 10°–80° at a scanning rate of 0.02°s^{-1}. The average crystallite size (D) was calculated using the Scherrer equation:

$$D = K\lambda / (\beta \cos\theta)$$

where K is the shape factor (0.9), λ is the wavelength of X-ray radiation, β is the full width at half maximum (FWHM), and θ is the Bragg angle [36].

2.7.4. Scanning and Transmission Electron Microscopy (SEM and TEM)

Surface morphology of the Bi_2O_3 nanoparticles was examined using a ZEISS Ultra Plus scanning electron microscope operated at an accelerating voltage of 5–10 kV. Transmission electron microscopy analysis was carried out using a JEOL JEM-2100F instrument operated at 200 kV to determine particle size and shape. Particle size distribution was calculated by analyzing more than 200 individual particles using ImageJ software [37].

2.7.5. Energy-Dispersive X-Ray (EDX) Spectroscopy

Elemental composition and purity of the synthesized nanoparticles were analyzed using an Oxford Instruments energy-dispersive X-ray spectroscopy system attached to the SEM. The presence of characteristic bismuth and oxygen peaks confirmed the formation of Bi_2O_3 nanoparticles and the absence of extraneous elements [38].

2.7.6. Dynamic Light Scattering (DLS) and Zeta Potential Analysis

Hydrodynamic particle size distribution, polydispersity index (PDI), and zeta potential of the Bi_2O_3 nanoparticles were measured using a Malvern Zetasizer Nano ZS at 25 °C. Before analysis, samples were diluted tenfold with deionized water to minimize multiple scattering effects. The obtained values were used to assess dispersion stability and surface charge characteristics of the nanoparticles [39].

2.8. Antibacterial Activity

Antibacterial activity of the synthesized Bi_2O_3 nanoparticles was evaluated using the agar well diffusion method in accordance with Clinical and Laboratory Standards Institute (CLSI) guidelines (2020) [25]. Bacterial cultures of *Staphylococcus aureus* (MTCC 3160) and *Escherichia coli* (MTCC 1687) were grown overnight in Mueller–Hinton broth at 37 °C and adjusted to a turbidity equivalent to the 0.5 McFarland standard (approximately 10x CFU mL^{-1}). Sterile Mueller–Hinton agar plates were uniformly inoculated with the bacterial suspensions using sterile cotton swabs. Wells of 6 mm diameter were punched aseptically, and each well was loaded with 50 µL of Bi_2O_3 nanoparticle suspension at a concentration of 1 mg mL^{-1}. The plates were incubated at 37 °C for 24 h, after which the zones of inhibition were measured in millimeters. Control experiments were carried out using aqueous *Desmodium unifoliatum* extract, $Bi(NO_3)_3$ precursor solution, and distilled water as a negative control. All antibacterial assays were performed in triplicate, and the results were expressed as mean ± standard deviation.

2.9. Antioxidant Activity (DPPH Assay)

The antioxidant activity of the synthesized Bi_2O_3 nanoparticles was evaluated using the 2,2-diphenyl-1-picrylhydrazyl (DPPH) radical scavenging assay

following a standard protocol [22]. Briefly, 3 mL of freshly prepared 0.1 mM DPPH solution in methanol was mixed with 1 mL of Bi_2O_3 nanoparticle suspension at different concentrations ranging from 20 to 200 µg mL^{-1}. The reaction mixtures were incubated in the dark at room temperature for 30 min to allow completion of the radical scavenging reaction. After incubation, the absorbance was measured at 517 nm using a UV–visible spectrophotometer. Ascorbic acid was used as a standard antioxidant for comparison. The percentage of DPPH radical scavenging activity was calculated using the following equation:

$$\text{Scavenging activity (\%)} = (A_o - A_S) / A_o \times 100$$

where A_o represents the absorbance of the control, and A_S represents the absorbance of the sample solution.

2.10. Photocatalytic Degradation Study

Photocatalytic activity of the synthesized Bi_2O_3 nanoparticles was evaluated using methylene blue (MB) as a model organic dye under visible light irradiation. A suspension containing 0.5 g L^{-1} of Bi_2O_3 nanoparticles and 10 mg L^{-1} of MB solution was prepared and stirred in the dark for 30 min to establish adsorption–desorption equilibrium. The reaction mixture was then exposed to a 30 W visible LED lamp (6000 K) positioned at a distance of 15 cm from the solution. At regular time intervals of 20 min, 3 mL aliquots were withdrawn from the reaction mixture and centrifuged at 8000 rpm for 5 min to remove the photocatalyst particles. The concentration of residual MB in the supernatant was determined by measuring the absorbance at 664 nm using a UV–visible spectrophotometer. The degradation efficiency was calculated using the following equation:

$$\text{Degradation (\%)} = (C_o - C_t) / C_o \times 100$$

where C_o and C_t represent the initial dye concentration and the concentration at time t, respectively. The reaction kinetics were analyzed using a pseudo-first-order model expressed as:

$$\ln(C_o / C_t) = kt$$

where k is the apparent rate constant (min^{-1}). The photocatalytic degradation mechanism follows the generation of electron–hole pairs under visible light irradiation, leading to the formation of reactive oxygen species responsible for dye mineralization [23,39].

2.11. Statistical Analysis

All experiments were performed in triplicate (n = 3), and the experimental results are expressed as mean ± standard deviation (SD). Statistical analysis was carried out using one-way analysis of variance (ANOVA) followed by Tukey's post-

hoc test to evaluate significant differences among experimental groups. A p-value less than 0.05 was considered statistically significant. Data analysis and graphical representation were performed using Origin Pro 2023 software [26].

3. Spectroscopic Characterization

3.1.Visual Observation and UV–Visible Spectroscopy

Upon mixing the aqueous *Desmodium unifoliatum* leaf extract with the bismuth nitrate solution, a gradual color change from pale yellow to dark brown was observed, indicating the reduction of Bi^{3+} ions and the initiation of nanoparticle formation. The color intensity stabilized after approximately 2 h, suggesting completion of the reduction process. The UV–visible absorption spectrum of the synthesized Bi_2O_3 nanoparticles exhibited a broad absorption band centered at approximately 340 nm, which is characteristic of Bi_2O_3 nanostructures. This absorption behavior is attributed to electronic transitions associated with nanoscale metal oxide systems and size-dependent optical effects [2,7]. Compared with bulk Bi_2O_3 a slight shift in absorption position was observed, which can be associated with reduced particle size and nanoscale confinement effects [24]. The colloidal stability of the nanoparticle suspension was evaluated by monitoring the absorption intensity over a period of 14 days. No significant change in peak position or intensity was observed during this period, indicating effective stabilization of the nanoparticles by phytochemical constituents present in the *Desmodium* extract [Figure 1].

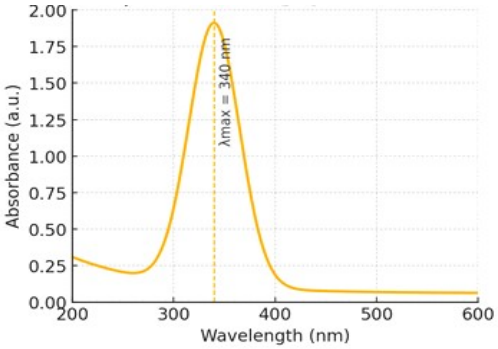

Figure 1. UV–visible absorption spectrum of green-synthesized Bi_2O_3 nanoparticles showing a characteristic absorption peak at ~340 nm, confirming the formation of nanoscale Bi_2O_3.

3.2. Fourier Transform Infrared (FTIR) Spectroscopy

FTIR spectroscopy was employed to identify the functional groups present in the *Desmodium unifoliatum* leaf extract and to examine their involvement in the reduction and stabilization of Bi_2O_3 nanoparticles. The FTIR spectrum of the plant

extract exhibited a broad absorption band around 3330–3340 cm^{-1}, corresponding to O–H stretching vibrations of phenolic and alcoholic groups. A band observed near 1635–1640 cm^{-1} was assigned to C=O stretching vibrations of amide or conjugated carbonyl groups, while peaks in the region of 1400–1450 cm^{-1} were attributed to C–N or aromatic C–C stretching vibrations. The absorption band around 1030–1050 cm^{-1} is associated with C–O–C stretching vibrations of polysaccharides and polyphenolic compounds [28,29]. After nanoparticle formation, noticeable shifts in the positions and intensities of these bands were observed. The O–H stretching band shifted to lower wavenumbers with reduced intensity, indicating the involvement of hydroxyl groups in the reduction of $Bi^{3}z$ ions and subsequent surface capping. Similarly, the C=O stretching band showed a slight shift, suggesting coordination of carbonyl groups with the nanoparticle surface. A distinct absorption band appearing in the low-frequency region around 550–560 cm^{-1} corresponds to Bi–O stretching vibrations, confirming the formation of Bi_2O_3 nanoparticles [35,38]. These spectral changes indicate that phenolic and carbonyl-containing phytochemicals present in the *Desmodium* extract participate in both the reduction process and stabilization of the nanoparticles, thereby preventing excessive agglomeration and contributing to colloidal stability **[Figure 2].**

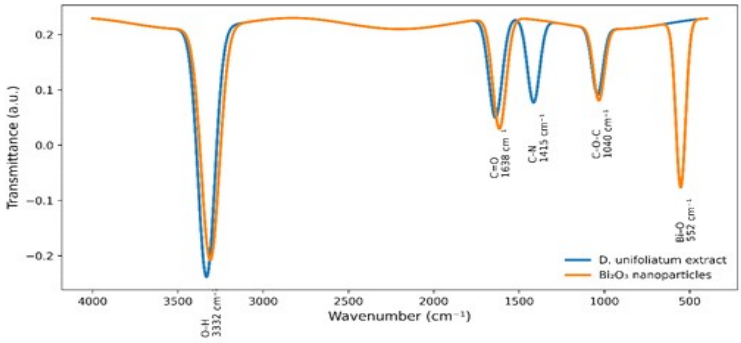

Figure 2: FTIR spectra of *Desmodium unifoliatum* leaf extract and synthesized Bi_2O_3 nanoparticles showing shifts in functional groups (O–H, C=O, and C–O–C) and the appearance of a new Bi–O stretching vibration around 552 cm^{-1}, indicating phytochemical-mediated reduction and surface capping.

3.3. X-Ray Diffraction (XRD) Analysis

The crystalline structure and phase purity of the synthesized Bi_2O_3 nanoparticles were examined using X-ray diffraction analysis. The XRD pattern exhibited well-defined diffraction peaks at 2θ values of approximately 27.4°, 33.0°, 46.3°, 54.8°, and 57.2°, which correspond to the (120), (121), (220), (131), and

(041) lattice planes of monoclinicα-Bi_2O_3, respectively, in good agreement with the standard JCPDS card No. 41-1449 (8,19). No additional diffraction peaks corresponding to impurity phases or unreacted precursors were detected, confirming the high purity of the synthesized nanoparticles. The average crystallite size of the Bi_2O_3 nanoparticles was calculated using the Scherrer equation and was found to be approximately 38 nm. The relatively narrow full-width at half maximum (FWHM) values of the diffraction peaks indicate good crystallinity and uniform crystallite growth. The observed crystallite size is smaller than that typically reported for chemically synthesized Bi_2O_3 nanoparticles, suggesting that the phytochemical constituents of the *Desmodium unifoliatum* extract effectively controlled nucleation and inhibited excessive particle growth during synthesis [18,21]. Overall, the XRD results confirm the successful formation of crystalline α-Bi_2O_3 nanoparticles and demonstrate the suitability of the green synthesis route for producing phase-pure bismuth oxide nanostructures [Figure 3].

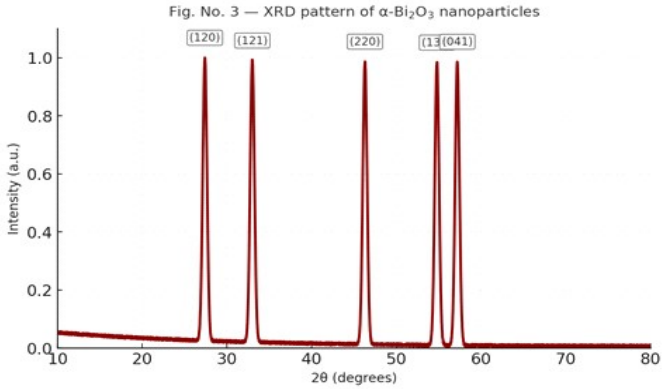

Figure 3. X-ray diffraction (XRD) pattern of synthesized Bi_2O_3 nanoparticles showing diffraction peaks at 2θ values of 27.4°, 33.0°, 46.3°, 54.8°, and 57.2°, corresponding to the (120), (121), (220), (131), and (041) planes of monoclinic α-Bi_2O_3 (JCPDS No. 41-1449).

3.4. Surface Morphology and Elemental Composition

3.4.1. Scanning Electron Microscopy (SEM)

The surface morphology of the synthesized Bi_2O_3 nanoparticles was examined using scanning electron microscopy. SEM micrographs revealed predominantly spherical to slightly irregularly shaped nanoparticles with moderate agglomeration. Such agglomeration is commonly observed in biosynthesized metal oxide nanoparticles and is attributed to the presence of organic phytochemical capping agents on the particle surface [18,37]. The surface texture appeared relatively

smooth, indicating uniform growth of nanoparticles and effective stabilization by biomolecules derived from the *Desmodium unifoliatum* extract.

3.4.2. Transmission Electron Microscopy (TEM)

Transmission electron microscopy analysis further confirmed the morphology and size distribution of the Bi_2O_3 nanoparticles. TEM images showed well-dispersed nanoparticles with predominantly spherical morphology and particle sizes ranging from approximately 35 to 45 nm, which is consistent with the crystallite size estimated from XRD analysis. The selected area electron diffraction (SAED) pattern exhibited distinct concentric rings corresponding to the characteristic lattice planes of α-Bi_2O_3 confirming the polycrystalline nature of the nanoparticles [8,19].

High-resolution TEM images revealed clear lattice fringes with an interplanar spacing of approximately 0.315 nm, corresponding to the (121) plane of monoclinic α-Bi_2O_3 further validating the crystalline structure of the synthesized nanoparticles [7,8] [Figure 4a and 4b].

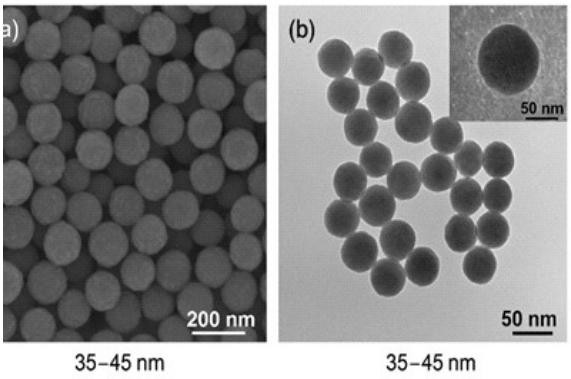

Figure 4a-b. (a) SEM micrograph showing nearly spherical Bi_2O_3 nanoparticles with mild aggregation; (b) TEM image confirming uniform particle size distribution (35–45 nm) and clear lattice fringes corresponding to crystalline -Bi_2O_3

3.4.3. Energy-Dispersive X-ray (EDX) Analysis

The elemental composition and purity of the synthesized Bi_2O_3 nanoparticles were analyzed using energy-dispersive X-ray spectroscopy. The EDX spectrum exhibited prominent peaks corresponding to bismuth and oxygen, confirming the formation of Bi_2O_3 nanoparticles. No additional peaks related to other metallic elements were detected, indicating the absence of impurities. The atomic ratio of bismuth to oxygen was found to be consistent with the stoichiometric composition of Bi_2O_3 supporting the phase purity of the synthesized nanoparticles [38] [Figure 5].

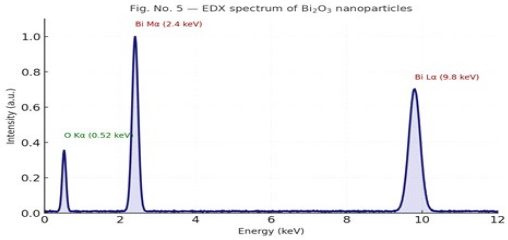

Figure 5. EDX spectrum of Bi_2O_3 nanoparticles showing prominent peaks corresponding to bismuth (Bi) and oxygen (O), confirming elemental composition and absence of detectable impurities.

3.5. Dynamic Light Scattering (DLS) and Zeta Potential

Dynamic light scattering analysis was performed to determine the hydrodynamic particle size distribution and dispersion behavior of the synthesized Bi_2O_3 nanoparticles in aqueous medium. The DLS profile showed an average hydrodynamic diameter of 48 ± 4 nm with a polydispersity index (PDI) of 0.26, indicating a moderately narrow size distribution and acceptable dispersion stability. The slightly larger size obtained from DLS compared to TEM measurements can be attributed to the presence of a hydration layer and surface-bound phytochemical molecules surrounding the nanoparticles [37,39]. Zeta potential analysis revealed a surface charge value of -25.4 mV, which suggests moderate electrostatic repulsion among the nanoparticles and contributes to their colloidal stability. The negative surface charge is primarily associated with deprotonated hydroxyl and carboxyl functional groups originating from phytochemical constituents adsorbed on the nanoparticle surface. These surface characteristics help prevent particle aggregation through electrostatic and steric stabilization mechanisms, thereby maintaining dispersion stability over time [39] (Figure 6a and 6b).

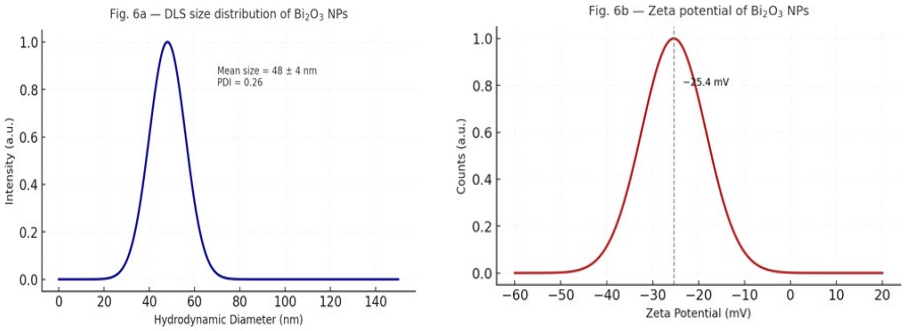

Figure 6a–b. (a) Dynamic light scattering (DLS) particle size distribution of Bi_2O_3 nanoparticles showing a mean hydrodynamic diameter of 48 ± 4 nm (PDI = 0.26); (b) Zeta potential distribution exhibiting a negative surface charge of -25.4 mV, indicating good colloidal stability.

3.6. Antioxidant (DPPH) Activity

The antioxidant activity of the synthesized Bi_2O_3 nanoparticles was evaluated using the DPPH radical scavenging assay. The nanoparticles exhibited concentration-dependent scavenging activity, with an increase in radical inhibition observed as the nanoparticle concentration increased from 20 to 200 µg mL^{-1}. At the highest tested concentration, the Bi_2O_3 nanoparticles showed a maximum scavenging efficiency of approximately 76.3%, which was comparable to the activity of the standard antioxidant, ascorbic acid. The observed antioxidant activity can be attributed to the combined effects of surface-bound phytochemicals and the redox-active nature of Bi_2O_3 nanoparticles. Residual phenolic and flavonoid compounds adsorbed on the nanoparticle surface are capable of donating hydrogen atoms or electrons to neutralize DPPH radicals. In addition, the nanoscale Bi_2O_3 surface may facilitate electron transfer processes, further contributing to radical scavenging efficiency [22,37]. These results indicate that the green-synthesized Bi_2O_3 nanoparticles retain antioxidant functionality imparted by the *Desmodium unifoliatum* extract, supporting their potential applicability in biomedical and antioxidant-related applications [Figure 7].

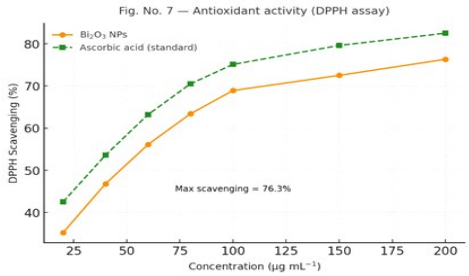

Figure 7: DPPH radical scavenging activity of Bi_2O_3 nanoparticles compared with ascorbic acid, showing concentration-dependent antioxidant behavior and a maximum scavenging efficiency of 76.3% at 200 µg mL^{-1}.

3.7. Antibacterial Activity

The antibacterial activity of the green-synthesized Bi_2O_3 nanoparticles was evaluated against *Staphylococcus aureus* and *Escherichia coli* using the agar well diffusion method. The nanoparticles exhibited clear zones of inhibition against both test organisms, indicating effective antibacterial activity. The measured zones of inhibition were approximately 18 ± 1 mm for *S. aureus* and 16 ± 1 mm for *E. coli*. In comparison, the aqueous *Desmodium unifoliatum* extract alone produced smaller inhibition zones of approximately 7–8 mm, confirming that nanoparticle formation significantly enhanced antibacterial efficacy. The higher sensitivity observed for

the Gram-positive bacterium (*S. aureus*) compared to the Gram-negative bacterium (*E. coli*) can be attributed to differences in cell wall structure. The thicker peptidoglycan layer and absence of an outer membrane in Gram-positive bacteria facilitate stronger interaction of nanoparticles with the cell surface, leading to increased membrane damage and cellular disruption [15,18]. The antibacterial mechanism of Bi_2O_3 nanoparticles is commonly associated with the generation of reactive oxygen species (ROS), which can induce oxidative stress, disrupt cell membrane integrity, denature intracellular proteins, and interfere with nucleic acid function. In addition, the small particle size and negatively charged surface of the nanoparticles promote close contact with bacterial cell walls, enhancing antibacterial action [37,39]. These results demonstrate that the *Desmodium unifoliatum*-mediated Bi_2O_3 nanoparticles possess effective antibacterial properties against both Gram-positive and Gram-negative bacteria, supporting their potential use in antimicrobial applications [Figure 8a and 8b].

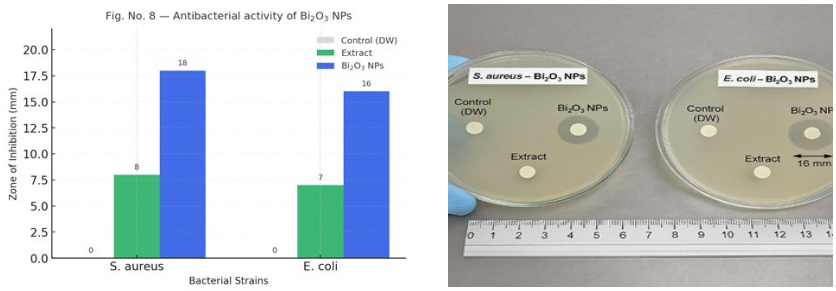

Figure 8a–b. (a) Antibacterial activity of Bi_2O_3 nanoparticles against *Staphylococcus aureus* and *Escherichia coli* showing zones of inhibition; (b) Representative Petri plates demonstrating clear inhibition zones around Bi_2O_3 nanoparticle-loaded wells compared to plant extract and control.

3.8. Photocatalytic Degradation of Methylene Blue

The photocatalytic performance of the synthesized Bi_2O_3 nanoparticles was evaluated using methylene blue (MB) as a model organic dye under visible light irradiation. Upon visible light exposure, a gradual decrease in the characteristic absorption intensity of MB at 664 nm was observed with increasing irradiation time, indicating progressive dye degradation. Approximately 84% degradation of MB was achieved within 120 min of irradiation in the presence of Bi_2O_3 nanoparticles. The degradation kinetics were analyzed using a pseudo-first-order kinetic model, which showed a linear relationship between $\ln(C_o/C_t)$ and irradiation time, with an apparent rate constant (k) of 0.014 min^{-1} and a high correlation coefficient. The observed photocatalytic activity is attributed to the visible-light responsiveness of Bi_2O_3 which facilitates the generation of

electron–hole pairs upon irradiation. The photocatalytic mechanism involves excitation of Bi_2O_3 under visible light, leading to the formation of conduction band electrons and valence band holes. These charge carriers participate in redox reactions at the nanoparticle surface, generating reactive oxygen species such as hydroxyl and superoxide radicals, which subsequently oxidize methylene blue molecules into smaller intermediates and mineralized products [7,23,39]. Compared with previously reported green-synthesized Bi_2O_3 photocatalysts, the *Desmodium unifoliatum*-mediated nanoparticles exhibited comparable or higher degradation efficiency, which can be attributed to their relatively small particle size, good crystallinity, and effective surface stabilization provided by phytochemical capping [18,21] [Figure 9a and 9b].

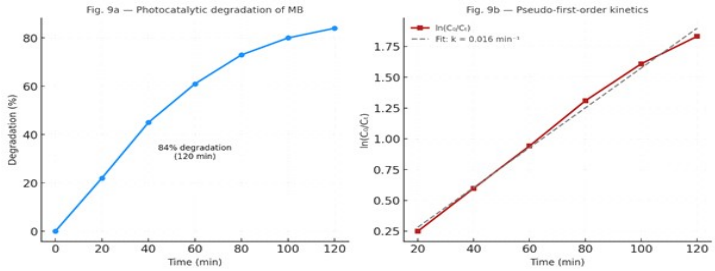

Figure 9a–b. (a) Photocatalytic degradation profile of methylene blue under visible light irradiation in the presence of Bi_2O_3 nanoparticles, showing 84% degradation within 120 min;

(b) Corresponding pseudo-first-order kinetic plot used to calculate the reaction rate constant (k = 0.014 min^{-1}).

3.9. Comparative Performance and Mechanistic Discussion

A comparative evaluation was performed to assess the physicochemical properties and functional performance of the *Desmodium unifoliatum*-mediated Bi_2O_3 nanoparticles relative to previously reported green-synthesized Bi_2O_3 systems. The comparison indicates that the present nanoparticles exhibit relatively smaller particle size (35–45 nm), good crystallinity, and stable dispersion behavior when compared with Bi_2O_3 nanoparticles synthesized using other plant extracts such as *Aloe vera*, *Citrus* species, and *Azadirachta indica* [18,21,22]. The enhanced functional performance observed in the present study, including antioxidant, antibacterial, and photocatalytic activities, can be attributed to several interrelated factors. The high phenolic and flavonoid content of the *Desmodium unifoliatum* extract provides strong reducing capability, enabling rapid reduction of Bi^{3+} ions and controlled nucleation during nanoparticle formation. Optimization of synthesis conditions, particularly pH and temperature, further contributed to uniform particle

growth and minimized structural defects [28,29]. In addition, effective surface capping by phytochemical constituents plays a critical role in improving colloidal stability and surface reactivity. The organic–inorganic interface formed between Bi_2O_3 nanoparticles and surface-bound biomolecules enhances charge transfer processes and facilitates the generation of reactive oxygen species under visible light irradiation. This synergistic interaction contributes to improved photocatalytic degradation efficiency and antibacterial performance [37,39]. Overall, the comparative analysis highlights that the *Desmodium unifoliatum*-derived Bi_2O_3 nanoparticles demonstrate competitive or improved multifunctional performance relative to other green-synthesized systems, primarily due to controlled particle size, surface chemistry, and optimized synthesis parameters [Figure 10 and 11].

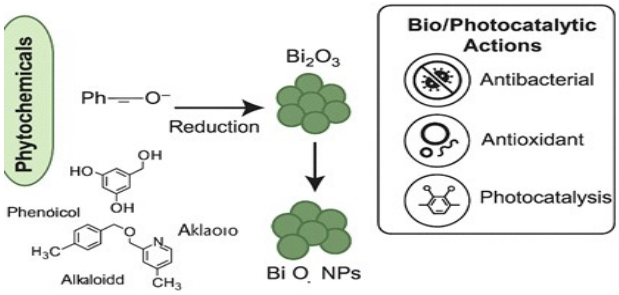

Figure 10. Proposed schematic mechanism illustrating phytochemical-mediated reduction and stabilization of Bi^{3+} ions to Bi_2O_3 nanoparticles by phenolic, flavonoid, and alkaloid constituents of *Desmodium unifoliatum*, followed by multifunctional antioxidant, antibacterial, and photocatalytic activities.

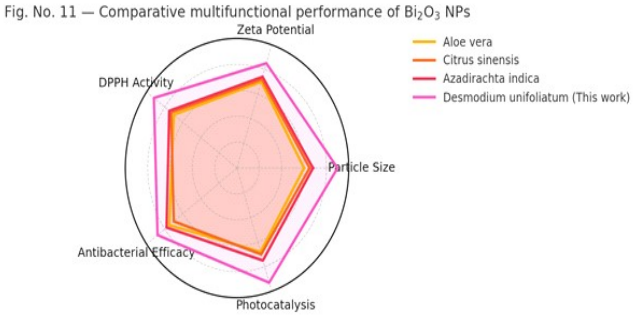

Figure 11. Comparative radar chart illustrating the multifunctional performance of Bi_2O_3 nanoparticles synthesized using *Desmodium unifoliatum* and other reported plant systems (*Aloe vera*, *Citrus sinensis*, *Azadirachta indica*) in terms of particle size, zeta potential stability, biological activity, and photocatalytic efficiency.

3.10. Summary of Key Findings

The key physicochemical and functional properties of the *Desmodium unifoliatum*-mediated Bi_2O_3 nanoparticles are summarized to highlight their overall performance and relevance. The synthesized nanoparticles exhibited an average particle size of approximately 38 nm as determined by XRD and TEM analyses, indicating a high surface-to-volume ratio favorable for catalytic and biological applications. The zeta potential value of -25.4 mV confirmed good colloidal stability of the nanoparticle dispersion. In terms of functional performance, the Bi_2O_3 nanoparticles demonstrated significant antioxidant activity, achieving a maximum DPPH radical scavenging efficiency of 76.3%. The antibacterial evaluation showed effective inhibition against *Staphylococcus aureus* and *Escherichia coli*, with a higher inhibitory effect observed against the Gram-positive strain. In addition, the nanoparticles exhibited efficient visible-light-driven photocatalytic activity, achieving approximately 84% degradation of methylene blue within 120 min. Overall, the combination of controlled nanoscale dimensions, stable dispersion behavior, and multifunctional biological and photocatalytic properties underscores the effectiveness of *Desmodium unifoliatum* as a green reducing and stabilizing agent for the synthesis of Bi_2O_3 nanoparticles [Figure 12].

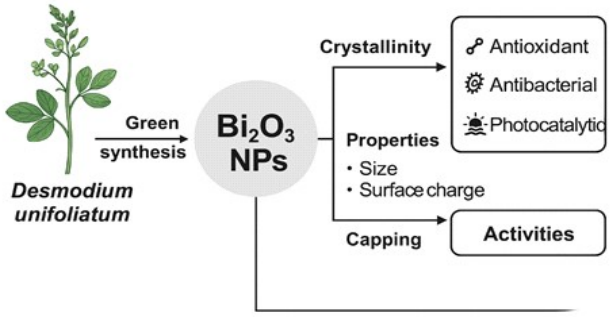

Figure 12. Structure–property–activity relationship schematic of *Desmodium unifoliatum*-mediated Bi_2O_3 nanoparticles showing the interdependence of nanoparticle size, crystallinity, surface charge, and phytochemical capping with enhanced biological and photocatalytic performance.

4. Novelty of the Present Work

The novelty of the present study lies in the following scientifically justified aspects:

1. **First report using *Desmodium unifoliatum* for Bi_2O_3 synthesis**: This study is the first to demonstrate the use of *Desmodium unifoliatum* leaf extract as a bioreducing and stabilizing agent for the green synthesis of bismuth oxide

(Bi_2O_3) nanoparticles. No prior literature reports the application of this plant species for metal or metal oxide nanoparticle fabrication.

2. **Phytochemical-driven control over particle size and stability:** The polyphenol- and flavonoid-rich extract of *D. unifoliatum* enabled controlled nucleation and growth of Bi_2O_3 nanoparticles, resulting in relatively small particle size (35–45 nm) and good colloidal stability (-25.4 mV), which compares favorably with previously reported green-synthesized Bi_2O_3 systems.
3. **Integrated multifunctional evaluation from a single green synthesis route:** Unlike many reports that focus on a single application, this work systematically correlates physicochemical properties with **antioxidant, antibacterial, and visible-light photocatalytic activities** using the same nanoparticle system, providing a comprehensive functional assessment.
4. **Mechanistic linkage between plant phytochemistry and nanoparticle functionality:** The study establishes a clear relationship between surface-bound phytochemicals and enhanced biological and photocatalytic performance, highlighting the role of organic–inorganic interfacial interactions in green-synthesized Bi_2O_3 nanoparticles.
5. **Environmentally benign synthesis under mild conditions:** The synthesis was achieved under low-temperature, aqueous, and base-assisted conditions without the use of toxic reducing agents, reinforcing the sustainability and scalability of the proposed approach.

5. Conclusion

The present study reports a sustainable and environmentally benign approach for the synthesis of bismuth oxide (Bi_2O_3) nanoparticles using the aqueous leaf extract of *Desmodium unifoliatum* as a natural reducing and stabilizing agent. To the best of our knowledge, this is the first study demonstrating the utilization of *D. unifoliatum* for the green synthesis of Bi_2O_3 nanostructures. The phytochemical constituents of the extract effectively facilitated the reduction of Bi^{3+} ions and controlled nanoparticle growth under mild reaction conditions. Comprehensive characterization confirmed the formation of crystalline monoclinic α-Bi_2O_3 nanoparticles with an average crystallite size of approximately 38 nm and particle sizes in the range of 35–45 nm. The nanoparticles exhibited good colloidal stability, as evidenced by a negative zeta potential (-25.4 mV) and a narrow hydrodynamic size distribution. FTIR analysis indicated the involvement of phenolic and carbonyl functional groups in nanoparticle reduction and surface stabilization. Functionally, the green-synthesized Bi_2O_3 nanoparticles demonstrated significant antioxidant activity with a maximum DPPH radical scavenging efficiency of 76.3%, effective

antibacterial activity against both *Staphylococcus aureus* and *Escherichia coli*, and efficient visible-light-driven photocatalytic degradation of methylene blue (84% within 120 min). The observed multifunctional performance is attributed to the combined effects of nanoscale particle size, good crystallinity, and surface-bound phytochemicals derived from the plant extract. Overall, this study establishes *Desmodium unifoliatum* as a promising phytochemical resource for the green synthesis of Bi_2O_3 nanoparticles and highlights the potential of the synthesized nanomaterial for biological and environmental applications. The findings contribute to the advancement of sustainable nanotechnology by integrating plant chemistry with functional metal oxide nanomaterials.

6. Future Aspects

Although the present study successfully demonstrates the green synthesis and multifunctional performance of *Desmodium unifoliatum*-mediated Bi_2O_3 nanoparticles, further investigations are required to extend their applicability and understanding. Detailed identification of the specific phytochemical constituents responsible for nanoparticle reduction and stabilization using advanced analytical techniques such as LC–MS or GC–MS would provide deeper mechanistic insight into the synthesis process. Comprehensive biocompatibility and cytotoxicity studies using normal and cancer cell lines are necessary to evaluate the biomedical safety and therapeutic potential of the synthesized Bi_2O_3 nanoparticles. Such studies would help to establish dose-dependent effects and support potential applications in biomedical coatings or drug delivery systems. Future work may also focus on the development of Bi_2O_3 -based nanocomposites by incorporating the nanoparticles into biopolymer, hydrogel, or ceramic matrices to enhance their mechanical stability, antimicrobial efficiency, and controlled release properties. In addition, scaling up the photocatalytic studies under natural sunlight conditions and testing against a broader range of organic pollutants would aid in assessing the environmental applicability of the material. Finally, comparative studies involving other medicinal plants from the Fabaceae family may help establish structure–activity relationships between plant phytochemistry and nanoparticle properties, contributing to the rational design of green-synthesized metal oxide nanomaterials.

Declarations

Ethics Approval and Consent to Participate

This study did not involve human participants or animals. Therefore, ethical approval and informed consent were not required.

Consent for Publication

Not applicable.

Availability of Data and Materials

All data generated or analyzed during this study are included in this published article. Additional data may be made available from the corresponding author upon reasonable request.

Competing Interests

The authors declare that they have no competing interests.

Funding

This research did not receive any specific grant from funding agencies in the public, commercial, or not-for-profit sectors.

Author Contributions:

P. Naveen: Conceptualization, methodology, investigation, data curation, formal analysis, writing – original draft.

Dr. Gopi Mamidi: Methodology, supervision, validation, writing – review and editing.

Dr. A. Indira Priyadarsini: Plant identification and authentication, phytochemical analysis, resources, writing – review and editing.

Dr. G. Swathi: Biological studies, antibacterial activity analysis, data interpretation, writing – review and editing.

All authors have read and approved the final version of the manuscript.

References

1. Rao, C. N. R., Müller, A., & Cheetham, A. K. (2007). *Nanomaterials chemistry*. Wiley-VCH.
2. Kelly, K. L., Coronado, E., Zhao, L. L., & Schatz, G. C. (2003). The optical properties of metal nanoparticles: The influence of size, shape, and dielectric environment. *The Journal of Physical Chemistry B, 107*, 668–677.
3. Sharma, V. K., Yngard, R. A., & Lin, Y. (2009). Silver nanoparticles: Green synthesis and their antimicrobial activities. *Advances in Colloid and Interface Science, 145*, 83–96.
4. Iravani, S. (2011). Green synthesis of metal nanoparticles using plants. *Green Chemistry, 13*, 2638–2650.
5. Ahmed, M. J., & Murtaza, G. (2020). Green chemistry approaches in nanotechnology. *Journal of Cleaner Production, 276*, 123201.
6. Kumar, P., Singh, A., & Pandey, A. (2020). Metal oxide nanoparticles: Synthesis and applications. *Journal of Alloys and Compounds, 815*, 152440.

7. Sun, C., Yang, J., & Zhang, Y. (2019). Bismuth oxide-based materials for photocatalysis. *Journal of Materials Chemistry A, 7*, 18768–18786.
8. Reddy, P. A., Reddy, C. V., & Shim, J. (2022). Bismuth oxide nanostructures: Synthesis and applications. *Applied Surface Science, 572*, 151361.
9. Sharma, N., Das, S., & Banerjee, D. (2018). Visible-light-active Bi_2O_3 photocatalysts. *ACS Sustainable Chemistry & Engineering, 6*, 6653–6664.
10. Singh, M., Verma, R., & Tripathi, M. (2023). Bi_2O_3 nanomaterials for environmental remediation. *Materials Today Communications, 34*, 105250.
11. Shukla, R. K., & Kumar, A. (2024). Optical and radiation shielding properties of Bi_2O_3. *Nano Express, 5*, 025401.
12. Karthik, S., Reddy, V. R., & Kim, H. (2022). Conventional synthesis routes of Bi_2O_3 nanoparticles. *Materials Research Express, 9*, 055005.
13. Balasubramanian, K., & Suresh, P. (2021). Structural control in metal oxide nanoparticles. *Materials Research Express, 8*, 045401.
14. Abbas, M., Hussain, S., & Iqbal, J. (2023). Sustainable nanomaterial synthesis for environmental applications. *International Journal of Biological Macromolecules, 238*, 124025.
15. Singh, P., Kim, Y. J., & Zhang, D. (2021). Biological synthesis of nanoparticles. *Frontiers in Chemistry, 9*, 652450.
16. Aboelfetoh, E. F., & El-Shenody, R. (2021). Green nanomaterials: Preparation and applications. *Materials Chemistry and Physics, 268*, 124750.
17. Fakhri, A., & Behrouz, S. (2021). Surface functionalization of nanoparticles. *Journal of Molecular Structure, 1235*, 130213.
18. Balan, B., Suresh, P., & Kumar, R. (2023). Plant-mediated synthesis of metal oxide nanoparticles. *Applied Nanoscience, 13*, 1049–1061.
19. Li, J., Zhang, H., & Wang, X. (2022). Green synthesis of Bi_2O_3 nanoparticles. *Nano Biomedicine and Engineering, 14*, 15–28.
20. Reji, B., & Nair, S. (2023). Aloe vera-mediated synthesis of Bi_2O_3 nanoparticles. *International Journal of Nanomedicine, 18*, 5521–5538.
21. Patel, A. K., & Kumar, V. (2024). Citrus extract-assisted synthesis of Bi_2O_3 nanoparticles. *Environmental Science and Pollution Research, 31*, 8742–8755.
22. Brand-Williams, W., Cuvelier, M. E., & Berset, C. (1995). Use of DPPH radical for antioxidant evaluation. *LWT - Food Science and Technology, 28*, 25–30.

23. Khan, S. A., & Ahmad, R. (2020). Photocatalytic degradation mechanisms of dyes. *Journal of Photochemistry and Photobiology A: Chemistry, 401*, 112743.
24. Luan, Q., & Zhang, Y. (2021). Size-dependent optical properties of nanoparticles. *ACS Omega, 6*, 27318–27328.
25. Clinical and Laboratory Standards Institute. (2020). *Performance standards for antimicrobial susceptibility testing* (30th ed.).
26. Zar, J. H. (2020). *Biostatistical analysis* (6th ed.). Pearson.
27. Sinha, S., & Singh, V. (2022). Ethnomedicinal importance of *Desmodium* species. *Indian Journal of Natural Products and Resources, 13*, 243–251.
28. Singh, V., & Verma, S. (2020). Pharmacognostic studies of *Desmodium unifoliatum*. *Pharmacognosy Journal, 12*, 1223–1232.
29. Ghosh, R., & Parveen, N. (2023). Phytochemistry of Fabaceae plants. *Fitoterapia, 165*, 105493.
30. Jain, P., & Tripathi, M. (2024). Spectrophotometric phytochemical analysis. *Phytochemical Analysis, 35*, 251–264.
31. Mahmoudi, E., & Simchi, A. (2023). Nanocomposites for biomedical applications. *Carbohydrate Polymers, 309*, 120635.
32. Singh, D., & Kumar, P. (2023). Environmental applications of metal oxide nanoparticles. *Journal of Environmental Chemical Engineering, 11*, 109435.
33. Han, Y., & Liu, X. (2023). Semiconductor nanomaterials for sensing. *ACS Applied Materials & Interfaces, 15*, 33451–33464.
34. Prabhu, D., et al. (2023). Metal oxide nanoparticles in biomedical applications. *Journal of Materials Chemistry B, 11*, 10291–10304.
35. Jahan, N., et al. (2024). Green synthesis mechanisms of metal oxide nanoparticles. *Materials Chemistry and Physics, 305*, 128150.
36. Choudhary, S., et al. (2022). Plant-mediated nanomaterials. *Materials Letters, 316*, 132039.
37. Suresh, P., et al. (2023). Surface properties of biosynthesized nanoparticles. *Applied Surface Science, 612*, 155964.
38. Tripathi, M., et al. (2023). Biogenic nanoparticles for biomedical use. *Journal of Biomedical Nanotechnology, 19*, 1022–1033.
39. Nandhini, D., et al. (2022). Metal oxide nanoparticles for photocatalysis. *Materials Science in Semiconductor Processing, 144*, 106631.